Research Paper

Empirical assessment of the critical time increment in explicit particulate discrete element method simulations

Masahide Otsubo, Catherine O'Sullivan *, Tom Shire

Department of Civil and Environmental Engineering, Imperial College London, United Kingdom

A B S T R A C T

This contribution considers the critical time increment (Δt_{crit}) to achieve stable simulations using particulate discrete element method (DEM) codes that adopt a Verlet-type time integration scheme. The Δt_{crit} is determined by considering the maximum vibration frequency of the system. Based on a series of parametric studies, Δt_{crit} is shown to depend on the particle mass (m), the maximum contact stiffness (K_{max}), and the maximum particle coordination number ($C_{N,max}$). Empirical expressions relating Δt_{crit} to m, K_{max}, and $C_{N,max}$ are presented; while strictly only valid within the range of simulation scenarios considered here, these can inform DEM analysts selecting appropriate Δt_{crit} values.

1. Introduction

Particulate discrete element modelling (DEM) is well established as a research tool in science in general, and in geomechanics in particular; there has been a consistent increase in the number of DEM-related publications published each year over the past 20–25 years [1,2]. Understandably the emphasis in DEM-related publications has been on application of DEM to simulate physical systems [3], and associated developmental work focussing on implementation of contact models (e.g. [4]), simulating particle crushing, boundary conditions, etc. As is the case with any numerical method, such application orientated research should be supported by studies that examine the method itself, considering issues relating to accuracy (e.g. [5]) and numerical stability (e.g. [6,7]). This contribution specifically considers the issue of numerical stability, and applies eigenmode analyses to a database of DEM simulations to show how the particle characteristics, packing and stress level influence the critical time increment calculated from consideration of the maximum eigenfrequency. The paper includes a background section that discusses the issue of numerical stability in particulate DEM prior to introducing the analysis approach adopted. The results of the eigenmode analysis are then presented and followed by an overall synthesis that considers the effect of packing density, particle size distribution, particle inertia, coordination number and contact stiffness on the critical time increment.

2. Background

As outlined by Hanley and O'Sullivan [5] the second order velocity-Verlet integration scheme has been adopted in a number of DEM codes that are used in geomechanics applications including LAMMPS [8], LIGGHTS [9] and YADE [10] and the commercial codes PFC2D/3D use a related Verlet-based scheme [11]. This numerical method is conditionally stable, i.e. it is only when the time increment used is less than a threshold value (the critical time step, Δt_{crit}) that small perturbations in the initial data will give small changes in the final solution (e.g. [12]). Two approaches are used in the literature to determine Δt_{crit} for DEM simulations; the first is based on the oscillation period of a single degree of freedom system, while the second uses the Rayleigh wave speed.

In their initial description of the discrete element method Cundall and Strack [13] estimated Δt_{crit} by considering a single degree of freedom system of a mass m connected to the ground by a spring K, giving:

$$\Delta t_{crit,SDOF} = 2\sqrt{m/K} \tag{1}$$

Developing this idea, Hart et al. [14] suggest:

$$\Delta t_{crit,Hart} = 2\alpha\sqrt{\frac{m_{min}}{2K_{max}}} \tag{2}$$

where m_{min} is the minimum mass and K_{max} is the largest normal or tangential contact stiffness, α is a user specified parameter that accounts for the presence of multiple contacts for each mass; Hart et al. recommend $\alpha = 0.1$, i.e. $\Delta t_{crit,Hart} = 0.14\sqrt{\frac{m_{min}}{K_{max}}}$. Using these ideas and following a parametric study on monodisperse samples, Tsuji

* Corresponding author at: Dept. Civil and Environmental Engineering, Room 501, Skempton Building, Imperial College London, London SW7 2AZ, United Kingdom.
E-mail address: cath.osullivan@imperial.ac.uk (C. O'Sullivan).

et al. [15] adopted $\Delta t_{crit,Tsuji} = \frac{\pi}{5}\sqrt{\frac{m}{K}} = 0.63\sqrt{\frac{m}{K}}$. Simple DEM models use linear contact models where a constant spring stiffness is applied to all contacts and K is constant, however many researchers use a Hertzian contact model that uses a non-linear force-deformation relationship at the contacts to account for the variation in contact area with contact force. Referring to Johnson [16], in the contact normal direction the incremental (i.e. tangent) contact spring stiffness ($K_{N,Hertz}$) is then

$$K_{N,Hertz} = \frac{G\sqrt{2\tilde{R}}}{(1-\nu)}\sqrt{\delta} \qquad (3)$$

where G is the particle shear stiffness, ν is the particle Poisson's ratio, δ is the contact overlap and $\tilde{R} = \frac{2R_1 R_2}{R_1+R_2}$, R_1 and R_2 being the radii of the two contacting particles. The dependency on δ means there will be a range of spring stiffnesses in a DEM model at any given time and $K_{N,max}$ will vary during a simulation. This complicates application of Eq. (1). Jensen et al. [17] report a modified version of Eq. (1) that is considered in the LS-DYNA DEM code:

$$\Delta t_{crit,Cundall} = 0.2\pi\sqrt{\frac{m_{min}}{\frac{E}{3(1+2\nu)}\beta}} \qquad (4)$$

where E is the particle Young's modulus and β is a stiffness penalty parameter that is typically between 0.1 and 0.001. Tu and Andrade [18] argue that Δt_{crit} associated with rotational motion is critical and so

$$\Delta t_{crit,Tu} = 2\sqrt{\frac{2m_{min}}{5K_T}} = 1.2\sqrt{\frac{m_{min}}{K_T}} \qquad (5)$$

where K_T is the tangential spring stiffness.

In the PFC codes [19] a critical time step is found for each body by considering both rotational and translational motion to be uncoupled and calculating the ratios $\sqrt{m/k_{tran}}$ and $\sqrt{I/k_{rot}}$ where m and I are the mass and moment of inertia respectively. The translational and rotational stiffnesses (k_{tran} and k_{rot}) are determined by considering the diagonal terms of the contact stiffness matrix at each contact and then summing the contributions from all the contacts assuming the degrees of freedom to be uncoupled. The final critical time step is taken to be the minimum of all the ratios $\sqrt{m/k_{tran}}$ and $\sqrt{I/k_{rot}}$ computed for all degrees of freedom of all bodies. As individual contacts are considered this approach can be applied to Hertzian contacts. Referring to Serra et al. [20], who use a similar approach, this type of implementation is based on Gerschgorin's theorem as outlined by Underwood [21].

Where a Hertizan contact model is used, a number of authors argue that estimates of Δt_{crit} based on Eq. (1) are not valid. For example Boac et al. [22] and Li et al. [23] argue that this approach is inapplicable because the contact model is non-linear. Thornton [24] cited [25] to suggest that the Rayleigh wave speed determines the time step. Li et al. [23] give the following expression for the Rayleigh time step (T_R) (also cited in [17,22,26]):

$$T_R = \frac{\pi R \sqrt{\frac{\rho}{G}}}{0.1631\nu + 0.8766} \qquad (6)$$

where ρ is the particle density. Li et al. and Boac et al. [22] specify that R is the average particle radius (R_{ave}); when the same expression is given by Kremmer and Favier [27] and Kafui et al. [28], R is taken to be the minimum particle radius (R_{min}). Li et al. [23] justify this approach for estimating the critical time increment by arguing that it can be assumed that all of the energy in the system is transferred by Rayleigh waves, while Guo et al. [29] explain that this approach considers the time taken for a Rayleigh wave to pass a sphere in a single time increment.

As noted by Burns and Hanley [7] it is clear that application of these different approaches will give different time step values. Whichever approach is used it seems that users view the calculated Δt_{crit} values to be an estimate. As already stated Hart et al. [14] and Tsuji et al. [15] use experience/empirical considerations to apply a factor to Eq. (1). Boac et al. [30] state that in practice some fraction of T_R is used, and suggest this fraction should be 0.2–0.4, with the higher number being more suited to lower coordination numbers. Jensen et al. [17] state that for stability the minimum of the critical time increment calculated using T_R, and Eq. (4) should be multiplied by a factor of 0.2 (they also consider a third approach that takes particle velocity into account). Itasca [19] apply a default factor of 0.8 to their calculated Δt_{crit} and this factor can also be user-specified.

Note that while Thornton [24] also considered artificially increasing the particle density (density scaling) to increase the critical time step, this has consequences for the inertial number and the maximum strain rate that can be applied while maintaining quasi static conditions [31,32] and so density scaling is neither used nor recommended here.

3. Eigenvalue analysis

Stability of explicit time integration approaches applied to multi-degree of freedom systems is also a concern in dynamic finite element analysis. Belytschko et al. [12] state that for a system of constant strain elements

$$\Delta t_{crit,CS} = \frac{2}{\omega_{max}} \leqslant \min_{ele}\frac{2}{\omega_{ele}} = \min_{ele}\frac{l_{ele}}{c_{ele}} \qquad (7)$$

where ω_{max} is the maximum frequency of the linearized system, ω_{ele} is the frequency of element ele, l_{ele} is a characteristic length of element ele and c_{ele} is the current wave speed in element ele. Eq. (7) clearly links to the approaches used to determine Δt_{crit}; DEM analysts are implicitly relating the ratio $\sqrt{m/K}$ to ω_{ele}, while consideration of the Rayleigh wave speed relates to the ratio $\frac{l_{ele}}{c_{ele}}$. There is however a basic conceptual difference in the two approaches; the Cundall/Hart SDOF-based approach considers the system to be comprised of rigid bodies connected by springs, while the Rayleigh-wave-based approach considers the particles themselves to be elastic.

O'Sullivan and Bray [6] argued that the particles in a DEM simulation are analogous to the nodes in a finite element model, while the contacts are roughly equivalent to the elements. This conceptual model of a granular material is used in implicit discrete element method formulations such as the particulate form of discontinuous deformation analysis (DDA) as outlined in [11]. O'Sullivan and Bray [6] outlined that if it is assumed that linear stability analysis also holds for non-linear cases, then the maximum stable time increment (Δt_{crit}) is a function of the eigenvalues of the current stiffness matrix (e.g. [36,37]). As acknowledged by Tu and Andrade [18], the maximum frequency, ω_{max}, is related to the maximum eigenvalue (λ_{max}) of the $\mathbf{M}^{-1}\mathbf{K}$ matrix as

$$\omega_{max} = \sqrt{\lambda_{max}} \qquad (8)$$

O'Sullivan and Bray estimated the maximum eigenvalue of the system using the following expression which is an extension of Rayleigh's theorem ([36]):

$$\lambda_{max} \leqslant \lambda_{max}^{ele} \qquad (9)$$

where λ_{max}^{ele} is the maximum eigenvalue of the $\mathbf{M}^{ele-1}\mathbf{K}^{ele}$ matrix for element "ele", ($\mathbf{M}^{ele}$ = element mass matrix, $\mathbf{K}^{ele}$ = element stiffness matrix). An estimate for the critical time increment can then be made by applying Eq. (7), once λ_{max}^{ele} is known, and O'Sullivan and

Bray [6] presented expressions for element stiffness matrices for various lattice configurations. O'Sullivan and Bray considered each contact to be an element and assumed the mass assigned to the contact to be simply the particle mass divided by the coordination number. For the lattice packings they considered both the mass and the particle coordination numbers were uniform. O'Sullivan and Bray showed that Δt_{crit} reduced with increasing coordination number and that considering the rotational degree of freedom reduced Δt_{crit}. Their data indicated that for 3D analyses $\Delta t_{crit,OSB} \leqslant 0.17\sqrt{m/K}$; this supports the recommendation of Hart et al. [14] given in Eq. (2), but is significantly lower than the values recommended by Tsuji [15] and Tu and Andrade [18]. While O'Sullivan and Bray adopted an analytical approach, its general application must be revisited for a few reasons (i) they estimated the eigenvalues rather than directly calculating them (ii) they considered lattice packings and so their estimates not be generally applicable (iii) they made a very simple assumption in calculating the mass matrix.

With the original motivation of studying the dynamic response of granular materials a method was developed to construct the global mass and stiffness matrices for a DEM sample [38]; this method is applied here to directly calculate the eigenvalues for 3D DEM samples. For the 3D analyses considered here, each particle has 3 translational degrees of freedom and 3 rotational degrees of freedom and so the diagonal mass matrix ($\boldsymbol{M}$) includes the mass (m) and rotational inertia (I) values for each particle. Here the local contact stiffness matrix was created using the data available in the DEM model. The local contact stiffness matrix is a 12×12 element matrix; expressions for this matrix are given in the PFC manual [11] and the entries depend on the particle coordinates and contact stiffnesses. The element contact stiffness matrix, $\bar{k}_{ij}$, connecting particles (nodes) i and j is created in the global coordinate system and the degrees of freedom associated with node i are given by $[u_{i,x}, u_{i,y}, u_{i,z}, \theta_{i,x}, \theta_{i,y}, \theta_{i,z}]$ where $u_{i,s}$ is the translational displacement in direction s and $\theta_{i,s}$ is the rotation about axis s. The corresponding terms along the diagonal of the nodal mass matrix are $[m\,m\,m\,I\,I\,I]$ where m and I are the particle mass and rotational inertia, respectively. For clarity a representative element stiffness matrix for a contact normal orientated along the x-axis is given here as:

As there is no torsional resistance at the contacts where the simplified Hertz-Mindlin model considered here is used, the terms in k_{ij}^{nx} relating to the $\theta_{i,x}$ and $\theta_{j,x}$ degrees of freedom are zero. Once the k_{ij} terms are known the global stiffness matrix ($\boldsymbol{K}$) can be created using conventional stiffness matrix assembly techniques described in e.g. [33,34,35].

For the analyses presented here, the parameters required to construct the local stiffness matrix (particle coordinates, contact orientations and contact overlap) were obtained from the DEM sample configurations as described below. The normal spring stiffnesses were calculated using Eq. (3) and for the simplified Hertz-Mindlin (HM) model used here the tangential stiffness was:

$$K_T = \frac{2(1-\nu)}{2-\nu} K_N \tag{11}$$

For a sample composed of N_p particles, there are $6 \times N_p$ degrees of freedom; for the systems considered here $\boldsymbol{K}$ consisted of up to $355{,}098 \times 355{,}098$ elements. Where applicable, the particle–boundary contacts were also included in $\boldsymbol{K}$.

The eigenvalue decomposition was achieved by solving:

$$(\boldsymbol{K} - \lambda\boldsymbol{M})\phi = 0 \tag{12}$$

where λ are the eigenvalues and ϕ are the eigenvectors; each eigenvalue λ_i is associated with a particular eigenvector ϕ_i, and there are $6 \times N_p$ eigenvalues. Here, built-in MATLAB functions (MathWorks, 2015) were used to obtain the eigenvalues and eigenvectors. As before Eq. (7) relates ω_{max} and λ_{max} and

$$\Delta t_{crit,eig} = \frac{2}{\omega_{max}}. \tag{13}$$

4. Validation

Two approaches were adopted to validate the implemented eigenvalue decomposition approach. In the first case lattice packings were considered and the calculated $\Delta t_{crit,eig}$ values were compared with the values given by O'Sullivan and Bray [6]. O'Sullivan and Bray assumed $K_N = K_T$, however for the more general case of $K_N \neq K_T$, for the simple cubic packing when rotational degrees of freedom are omitted:

$$
k_{ij}^{nx} =
\begin{bmatrix}
K_N & & & & & & & & & & & \\
0 & K_T & & & & & & & & & & \\
0 & 0 & K_T & & & & & & & & & \\
0 & 0 & 0 & 0 & & & \text{symmetry} & & & & & \\
0 & 0 & -K_T R & 0 & K_T R^2 & & & & & & & \\
0 & K_T R & 0 & 0 & 0 & K_T R^2 & & & & & & \\
-K_N & 0 & 0 & 0 & 0 & 0 & K_N & & & & & \\
0 & -K_T & 0 & 0 & 0 & -K_T R & 0 & K_T & & & & \\
0 & 0 & -K_T & 0 & K_T R & 0 & 0 & 0 & K_T & & & \\
0 & 0 & 0 & 0 & 0 & 0 & 0 & 0 & 0 & 0 & & \\
0 & 0 & K_T R & 0 & K_T R^2 & 0 & 0 & 0 & K_T R & 0 & K_T R^2 & \\
0 & K_T R & 0 & 0 & 0 & K_T R^2 & 0 & -K_T R & 0 & 0 & 0 & K_T R^2
\end{bmatrix}
\tag{10}
$$

$$\Delta t_{crit} = 2\sqrt{\frac{m}{4k_N + 8k_T}} \tag{14}$$

and when rotation is included

$$\Delta t_{crit} = \min\left(2\sqrt{\frac{m}{4k_N + 8k_T}}, 2\sqrt{\frac{m}{20k_T}}\right) \tag{15}$$

Eqs. (14) and (15) reduce to the expressions in O'Sullivan and Bray when $K_N = K_T$. Referring to Fig. 1, a DEM model was created to consider a simple cubic (SC) sample with 2272 spherical particles and a HM contact model (D = 2.54 mm, m = 1.913 × 10^{-5} kg, ρ = 2230 kg/m^3, interparticle friction coefficient (μ) = 0.2, G = 25 GPa and v = 0.2) with mixed periodic and rigid wall boundaries, subject to an isotropic stress of p' = 100 kPa. This stress state was attained via servo controlled compression involving all 6 boundaries. Rotation was included in the DEM analyses. Once the sample had equilibrated the contact data were extracted; for this homogeneous sample these data were uniform giving K_N = 1.34 × 10^6 and K_T = 1.19 × 10^6 N/m at each contact. The contact data were used to form the global stiffness matrix, K, and subsequent eigenvalue decomposition gave $\Delta t_{crit,eig}$ = 1.79 × 10^{-6}s. This compared with a value of 1.79 × 10^{-6} s obtained using Eq. (15).

A face-centered cubic (FCC) sample was also considered, where only translational motion was considered

$$\Delta t_{crit} = 2\sqrt{\frac{m}{8k_N + 16k_T}} \tag{16}$$

A DEM model of 3200 spherical particles with a FCC packing was then created with the same material parameters as for the cubic sample and rotation was deactivated in the DEM model. The sample configuration was similar to that illustrated in Fig. 1a for the SC case. An isotropic stress state of p' = 100 kPa was applied via servo-control as before. As the packing differed from the SC case so too did the contact forces and so extracting the contact data gave K_N = 9.50 × 10^5 N/m and K_T = 8.44 × 10^5 N/m at each contact. Eigenvalue analysis gave $\Delta t_{crit,eig}$ = 2.31 × 10^{-6}s, this value is slightly larger than the value obtained by application of Eq. (16), which gave Δt_{crit} = 1.94 × 10^{-6} s. Detailed examination could not provide a clear explanation for the difference values. When rotation is included

$$\Delta t_{crit} = \min\left(2\sqrt{\frac{m}{8k_N + 16k_T}}, 2\sqrt{\frac{m}{40k_T}}\right) \tag{17}$$

(Note that Eq. (17) does not reduce to the expression in O'Sullivan and Bray as there is an error in the original paper). The DEM simulation of the 3200 sphere FCC sample was repeated including rotation, the contact data were extracted to populate K and the subsequent eigenvalue analysis gave $\Delta t_{crit,eig}$ = 1.51 × 10^{-6} s, which is very close to the value of 1.51 × 10^{-6} s obtained using Eq. (17).

Further validation of the approach was taken by considering the triaxial compression of a FCC sample. An expression relating the peak strength of this sample to the interparticle friction coefficient (μ) was derived by Thornton [39]. Referring to Fig. 2a and b, two sets of DEM simulations were carried out. Both used a sample of 192 particles on a FCC lattice surrounded by periodic boundary conditions at all sides with the particle properties given above and an interparticle friction of μ = 0.2. For the first series of simulations rotation was suppressed. In both cases an isotropic stress of p' = 100 kPa was applied using servo-controlled compression involving all 3 pairs of periodic boundaries. The sample was then subject to quasi-static triaxial compression, where one normal stress ($\sigma'_{zz} = \sigma'_1$) was increased while maintaining the orthogonal normal stresses constant (i.e., $\sigma'_{yy} = \sigma'_{xx} = \sigma'_3$) using servo control involving the two pairs of lateral boundaries (positioned at x_{min} and x_{max} and y_{min} and y_{max}). A strain rate of $\dot{\varepsilon}_{zz}$ = 0.002 s^{-1} was used so that the inertial number I calculated according to [32] was 7.59 × 10^{-7}; as $I < 1 \times 10^{-3}$ a quasi-static condition was achieved. Four simulation time increments (Δt_{sim}) were considered: 2.0 × 10^{-6} s, 2.21 × 10^{-6} s, 2.22 × 10^{-6} s and 2.4 × 10^{-6} s. The Δt_{sim} values were selected to be slightly larger than and slightly smaller than the $\Delta t_{crit,eig}$ which was calculated to be 2.31 × 10^{-6} s for p' = 100 kPa. The energy balance of the system was also traced, by summing the various contributions to energy including strain energy, kinetic energy, frictional dissipation and boundary work (input energy). Ideally the net energy, E_{net} (=strain energy + kinetic energy + frictional dissipation − boundary work), should be 0. For the case where Δt_{sim} = 2.4 × 10^{-6} s is used the highly erratic response associated with numerical instability is absent, however energy is clearly not conserved (Fig. 2d). Referring to the load:deformation response given in Fig. 2c, where a Δt_{sim} = 2.22 × 10^{-6} s is used, the simulation is not obviously unsta-

Periodic boundary

Rigid walls

Z

X

Y

(a)

Input parameters

Initial particle coordinates:
Initial sphere centroid positions determined from lattice topology
Simple cubic:2272 spheres
FCC: 3200 spheres

Particle properties:
D=2.54 mm; ρ=2230 kg/m^3

Contact model:
Hertz-Mindlin: G=25 GPa; v=0.2, μ=0.2

Boundary conditions:
Rigid wall at z_{min}, z_{max}
Periodic boundary at x_{min}, x_{max}, y_{min}, y_{max}

Simulation details:
Isotropic stress of p'=100 kPa achieved via servo-controlled compression, moving all 6 boundaries
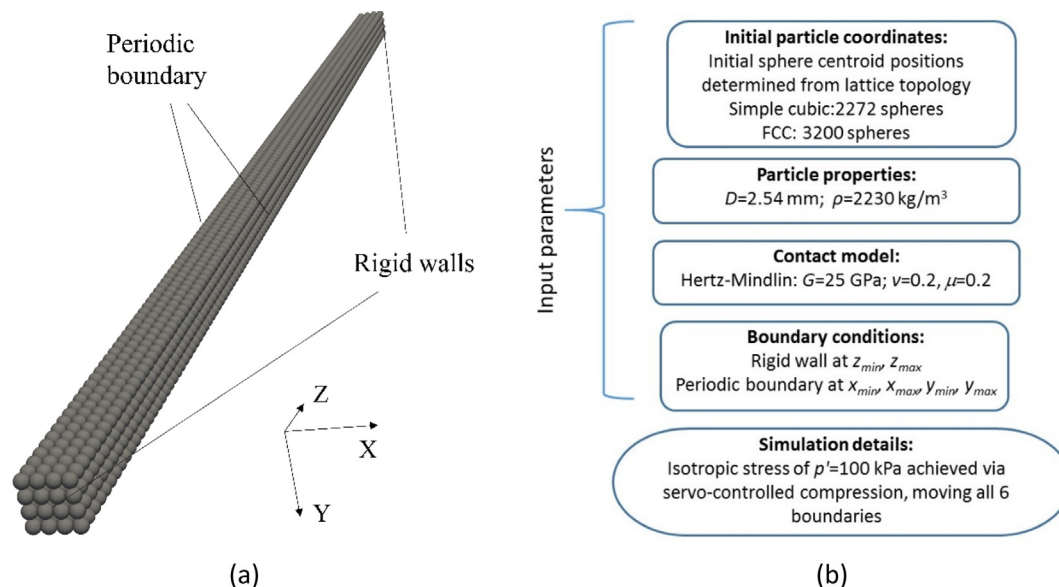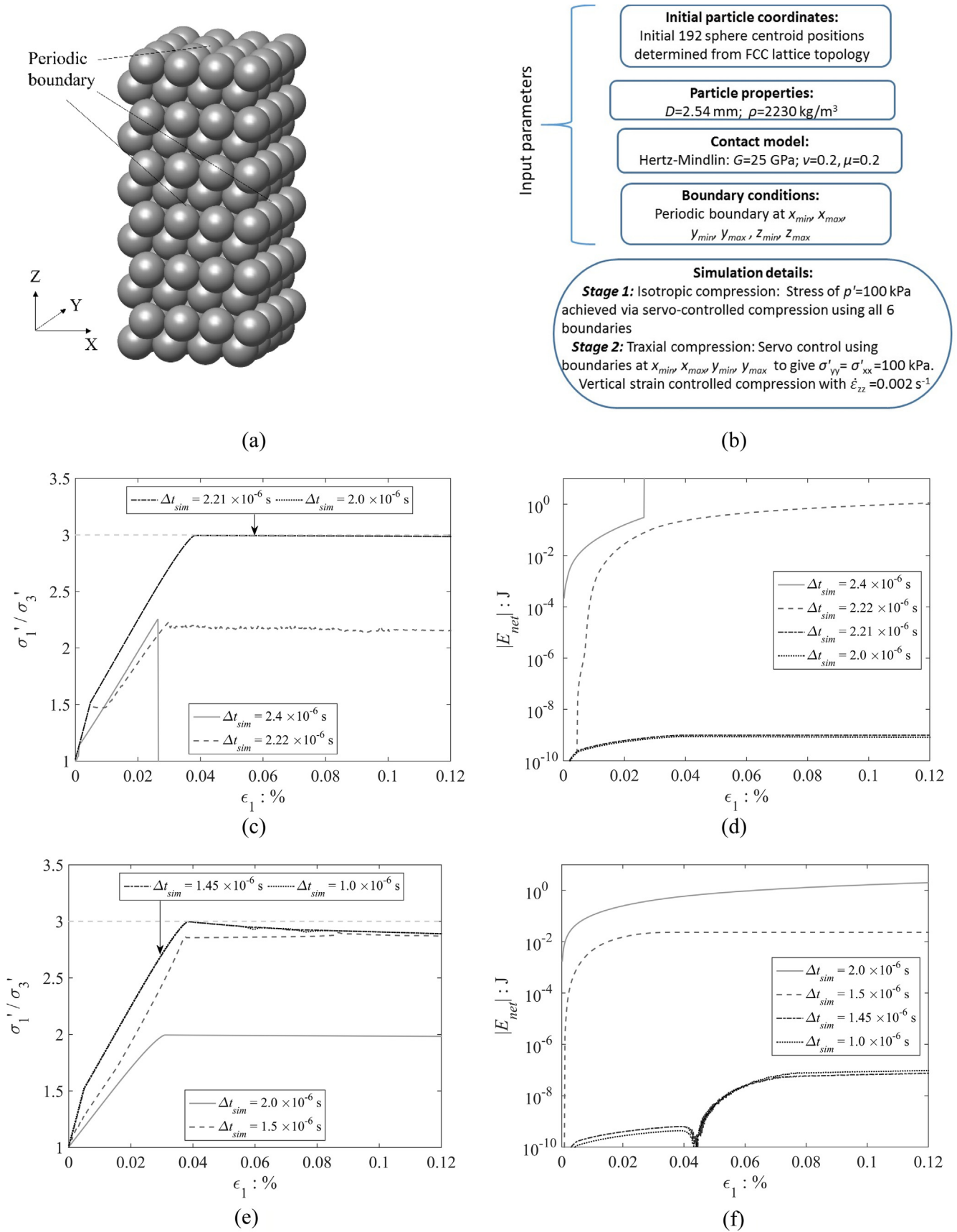
(b)

Fig. 1. DEM simulation of isotropic compression to provide contact data to validate the eigenvalue decomposition method to estimate the critical time steps. (a) Representative sample configuration (Simple cubic (SC) sample with 2272 spheres) and (b) flow chart for DEM simulation.

(a)

(b)

(c)

(d)

(e)

(f)

Fig. 2. Triaxial compression of FCC sample to validate eigenvalue decomposition method to estimate Δt_{crit}. (a) Graphical representation of sample, (b) simulation flow chart, (c) stress-strain response for translation only, (d) energy balance for translation only, (e) stress-strain response when rotation is allowed, and (f) energy balance when rotation is allowed.

ble; however, the peak stress ratio (σ_1/σ_3) is underestimated and again energy is clearly not conserved (Fig. 2d). However, when Δt_{sim} was reduced to 2.21×10^{-6} s, i.e. 96% of $\Delta t_{crit,eig}$, the peak stress ratio is accurately captured and there is no noticeable difference in the stress-strain response when Δt_{sim} is further reduced to 2.0×10^{-6} s. Referring to Fig. 2d for both cases of $\Delta t_{sim} = 2.0 \times 10^{-6}$ s or 2.21×10^{-6} s the net energy is of the order of $\times 10^{-9}$ J is small compared with the total energy in the system of the order of $\times 10^{-4}$ J. The simulations were repeated for the case where rotation was allowed; in this case four Δt_{sim} values were considered: 2×10^{-6} s, 1.5×10^{-6} s, 1.45×10^{-6} s and 1×10^{-6} s and $\Delta t_{crit,eig} = 1.51 \times 10^{-6}$ s. For $\Delta t_{sim} = 2 \times 10^{-6}$ s the stress-strain response is not obviously unstable, but the peak value is underestimated and there is a significant error in the net energy. Referring to Fig. 2e and f for the time increment just below the critical value, i.e. for $\Delta t_{sim} = 1.5 \times 10^{-6}$ s, the peak strength is underestimated by 0.1 and the energy balance is not satisfied. When Δt_{sim} is reduced to 1.45×10^{-6} s, i.e. to 96% of $\Delta t_{crit,eig}$, the peak value is accurately captured and the energy balance is effectively satisfied ($E_{net} < 1 \times 10^{-7}$ J). The need to reduce the time increment to be lower than the critical value calculated from eigenvalue decomposition of the (linearized) global stiffness matrix is acknowledged by Belytschko et al. [12]; they state that the stable time step should be multiplied by a factor between 0.8 and 0.98 to account for the destabilizing effects of non-linearities. Empirically it seems that use of $\Delta t_{stable} = 0.96 \Delta t_{crit,eig}$ is appropriate for both simulation cases.

5. Results

Three series of DEM simulations are considered here, and the simulation parameters are summarized in Tables 1–3. In all cases the simulations used a simplified Hertz-Mindlin (HM) contact model and a modified version of the LAMMPS code [8]. The simulations examined the effect of particle size, stress level and particle size distribution on the maximum eigenvalue and hence the critical time increment in DEM simulations.

As detailed in Table 1, and illustrated in Fig. 3a the first set of simulations considered cubic, isotropic samples of randomly placed monodisperse spheres enclosed by periodic boundaries on all sides. Referring to Fig. 3b, a series of five simulations were run in which the particle diameter (D) was systematically increased from 0.1 mm to 10 mm. Each sample contained 10,000 particles. Initially the samples were generated as non-contacting clouds of randomly placed particles; then a servo controlled compression was used to isotropically compress each sample to a mean effective stress of $p' = 50$ kPa with $\mu = 0.1$. A Young's modulus of 70 GPa, Poisson's ratio of 0.3 and particle density of 2670 kg/m^3 were used, giving a shear modulus of 27 GPa. For these simulations Δt_{sim} ranged from 4.44×10^{-7} s to 4.44×10^{-9} s. In all cases once the samples had equilibrated under the prescribed stress the contact data were extracted to form $\boldsymbol{K}$ and eigenvalue decomposition was carried out to determine $\Delta t_{crit,eig}$. Referring to Fig. 3c there is a linear relationship between $\Delta t_{crit,eig}$ and D when all other simulation parameters are unchanged. The distributions of per-particle coordination numbers are almost identical for the 5 cases considered

here as are the shapes of the contact force distributions. This finding has a theoretical basis: from Hertzian contact mechanics and effective medium theory (EMT) for a monodisperse sample (e.g. Yimsiri and Soga [40]) it can be shown that $K \propto D$. As $m \propto D^3$ then $\Delta t_{crit} \propto \sqrt{\frac{m}{K}}$ implies $\Delta t_{crit} \propto D$.

The second series of simulations again considered monodisperse spherical particles, with a sample configuration comprising a rectangular parallelepiped, bounding the longer dimensions, and two rigid wall boundaries contacting the smaller faces of the sample as illustrated in Fig. 4a. In this case three sample types were considered; samples with a face-centered cubic (FCC) lattice packing and randomly packed dense and loose samples. The simulation process is illustrated in Fig. 4b. In all cases typical properties of borosilicate glass ballotini were considered so that the particle density $\rho = 2230$ kg/m^3, the Young's modulus $E = 60$ GPa and particle Poisson's ratio $v = 0.2$, giving the shear modulus $G = 25$ GPa, and the particle diameter was 2.54 mm. These simulations were also considered in a study of stress wave propagation by [38] and are summarized in Table 2. As is often the case in DEM simulations the packing density was controlled by varying the inter-particle friction coefficient (μ) used during isotropic compression so that loose ($\mu = 0.4$) and dense ($\mu = 0$) randomly packed samples were considered (denoted RLP and RDP, respectively). The RLP samples had higher void ratios (e) and lower coordination numbers (C_N) than the RDP samples at the same confining pressure. The eigenvalue decomposition was performed for the FCC, RDP and RLP samples at four stress (p') levels: 10 kPa, 100 kPa, 1 MPa and 10 MPa. In all cases the tangential contact stiffness was activated by taking $\mu \neq 0$ and assuming no-slip condition at all contacts (conservative assumption). For each simulation once the sample attained equilibrium at the prescribed stress level contact data were extracted to populate $\boldsymbol{K}$ and an eigenvalue decomposition was then performed. The resultant $\Delta t_{crit,eig}$ values are given in Fig. 4c; the linear correlation observed indicates that $\Delta t_{crit,eig} \propto p'^{-1/6}$. This correlation is expected as for a Hertzian contact model adopting the assumptions used in EMT: $K_N \propto p'^{1/3}$ and $\Delta t_{crit} \propto 1/\sqrt{K_N}$. (Note that $K_T \propto K_N$ and so it also holds that $\Delta t_{crit} \propto 1/\sqrt{K_T}$). For the FCC sample, C_N is invariant for the simulation set; however, for the RLP and RDP samples, over the range of stresses considered, C_N varied by 1.38 and 0.93, respectively.

For the third series of simulations, the particle size distribution was systematically varied, while maintaining a constant minimum particle size of 0.1 mm, as illustrated in Fig. 5 and detailed in Table 3. Referring to Fig. 5a, 6 sample types, each with a linear particle size distribution were considered, so that the coefficient of uniformity of the samples (Cu) was systematically varied, where $Cu = D_{60}/D_{10}$ and X% of particles by mass are smaller than D_X. Fig. 5b illustrates PSDs for 4 additional samples with bi-linear PSDs with $Cu = 1.5$–1.6. The PSDs of each of the bi-linear samples follow a linear PSD with $Cu = 3$ to a diameter D_X, where X is specified by the number in the sample name (D_5 for BL5, D_{10} for BL10, etc.). In this case a cubic periodic cell was used (Fig. 5c). The simulation flow chart is given in Fig. 5d. The particles which were initially randomly placed and non-contacting, were isotopically compressed to a mean stress of $p' = 50$ kPa. Up to three coefficient of frictions (μ) were used for each grading considered (i.e. $\mu = 0.0$, 0.1, and 0.3) to give a range of void ratios, and the resultant samples are termed "dense", "medium" and "loose", respectively. As before, a simplified Hertz-Mindlin contact model was used with $v = 0.3$, $G = 27$ GPa and $\rho = 2670$ kg/m following [41] and so applying Eq. (1) with $R = R_{min}$ gives 1.07×10^{-7} s. Simulations were terminated when the mean normal stress reached the target level and the coordination number (the number of contacts per particle) remained constant for 20,000 simulation cycles. In all cases μ was increased to 0.3 and the samples were allowed to equilibrate;

Table 1
Monodisperse simulations.

D (mm)	Δt_{sim} (s)	T_R (s)	$K_{N,max}$ (N/m)	$\Delta t_{crit,eig}$ (s)
0.1	4.44×10^{-9}	5.34×10^{-8}	8.21×10^{4}	7.15×10^{-8}
0.3	1.33×10^{-8}	1.60×10^{-7}	2.40×10^{5}	2.14×10^{-7}
1	4.44×10^{-8}	5.34×10^{-7}	8.23×10^{5}	6.94×10^{-7}
3	1.33×10^{-7}	1.60×10^{-6}	2.65×10^{6}	2.16×10^{-6}
10	4.44×10^{-7}	5.34×10^{-7}	9.05×10^{6}	7.05×10^{-6}

Table 2
Monodisperse Simulation – vary p'.

Sample	p' (MPa)	μ	e	$C_{N,mean}$	$C_{N,max}$	Δt_{sim} (s)	T_R (s)	$K_{N,max}$ (N/m)	$\Delta t_{crit,eig}$ (s)
FCC	0.01	0	0.353	12.0	12	1.10×10^{-7}	1.31×10^{-6}	4.41×10^5	2.21×10^{-6}
	0.1		0.353	12.0	12			9.50×10^5	1.51×10^{-6}
	1		0.351	12.0	12			2.05×10^6	1.03×10^{-6}
	10		0.341	12.0	12			4.40×10^6	7.02×10^{-7}
R0	0.01	0	0.545	5.96	11			1.08×10^6	2.21×10^{-6}
	0.1		0.544	6.08	11			2.35×10^6	1.51×10^{-6}
	1		0.539	6.36	12			4.78×10^6	1.02×10^{-6}
	10		0.516	6.93	12			9.62×10^6	7.02×10^{-7}
R04	0.01	0.4	0.688	4.09	9			1.18×10^6	2.24×10^{-6}
	0.1		0.687	4.40	9			2.29×10^6	1.49×10^{-6}
	1		0.680	4.85	9			4.59×10^6	1.03×10^{-6}
	10		0.652	5.47	10			9.05×10^6	7.13×10^{-7}

Table 3
Polydisperse simulations.

PSD shape	Cu	Number of particles	μ	e	$C_{N,mean}$	$C_{N,max}$	$K_{N,max}$ (N/m)	$\Delta t_{crit,eig}$ (s)
Linear	1	10,000	0.0	0.566	6.06	11	7.84×10^4	7.18×10^{-8}
			0.1	0.666	5.22	10	8.21×10^4	7.15×10^{-8}
			0.3	0.730	4.45	9	8.05×10^4	7.16×10^{-8}
Linear	1.2	8262	0.0	0.558	5.99	12	9.94×10^4	5.99×10^{-8}
			0.1	0.651	5.17	12	9.61×10^4	5.69×10^{-8}
			0.3	0.714	4.32	10	1.03×10^5	6.06×10^{-8}
Linear	1.5	9313	0.0	0.527	5.83	17	1.30×10^5	6.39×10^{-8}
			0.1	0.607	4.89	14	1.32×10^5	6.28×10^{-8}
			0.3	0.659	3.88	14	1.42×10^5	6.06×10^{-8}
Linear	2	12,115	0.0	0.467	5.48	30	1.72×10^5	3.43×10^{-8}
			0.1	0.523	4.42	25	1.98×10^5	3.81×10^{-8}
			0.3	0.555	3.38	22	2.42×10^5	3.58×10^{-8}
Linear	3	22,600	0.0	0.382	5.06	92	2.74×10^5	2.24×10^{-8}
			0.1	0.426	3.73	79	3.43×10^5	1.50×10^{-8}
			0.3	0.455	2.53	59	3.86×10^5	1.88×10^{-8}
Linear	4.5	44,821	0.0	0.320	4.78	297	4.23×10^5	1.05×10^{-8}
			0.1	0.356	3.39	208	4.79×10^5	6.82×10^{-8}
			0.3	0.384	2.13	152	5.59×10^5	1.05×10^{-8}
Linear	6	59,183	0.0	0.265	4.58	639	5.67×10^5	6.63×10^{-9}
			0.1	0.292	3.23	517	1.04×10^6	7.82×10^{-9}
			0.3	0.314	1.96	332	1.11×10^6	5.86×10^{-9}
Bi-linear (BL5)	1.5	18,632	0.0	0.448	5.73	17	7.84×10^4	5.75×10^{-8}
			0.3	0.519	3.89	13	8.21×10^4	5.54×10^{-8}
Bi-linear (BL10)	1.5	19,915	0.0	0.442	5.66	16	9.94×10^4	5.54×10^{-8}
			0.3	0.506	3.87	15	9.61×10^4	5.38×10^{-8}
Bi-linear (BL15)	1.6	24,757	0.0	0.440	5.54	17	1.72×10^5	5.28×10^{-8}
			0.3	0.500	3.74	14	1.98×10^5	5.19×10^{-8}
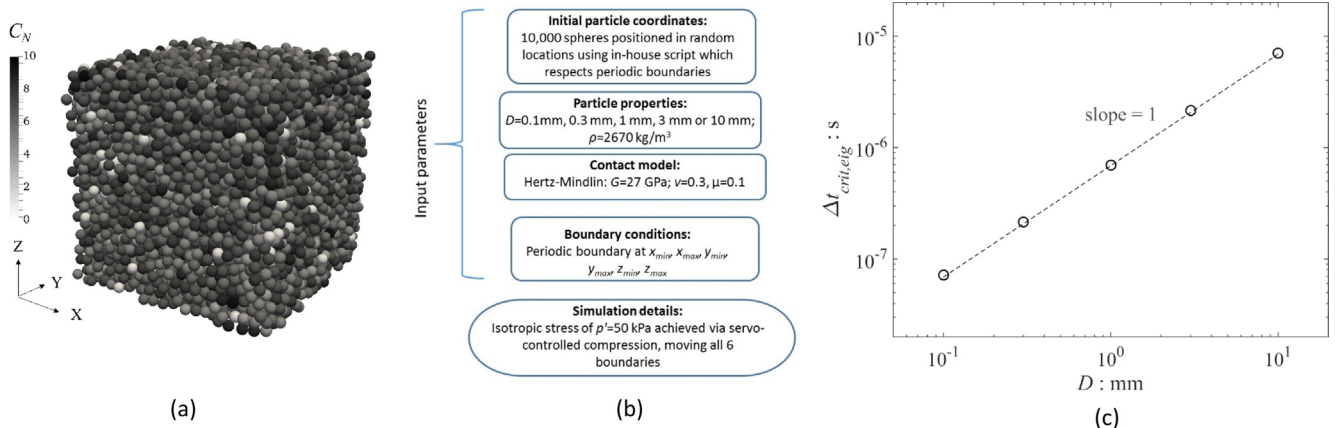
Fig. 3. Influence of particle inertia on $\Delta t_{crit,eig}$. (a) Simulation configuration, (b) simulation flow chart, and (c) variation in $\Delta t_{crit,eig}$ with particle diameter for medium-dense monodisperse samples at p' = 50 kPa.
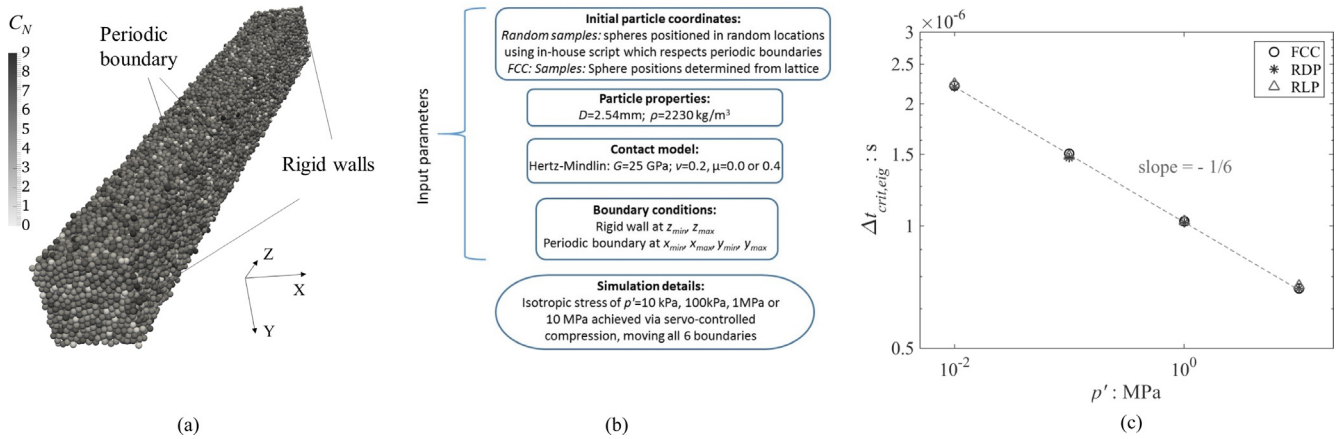
Fig. 4. Monodisperse samples with particle diameter = 2.54 mm. (a) Simulation configuration: particles coloured by particle coordination number (C_N), (b) simulation flow chart, and (c) variation in $\Delta t_{crit,eig}$ with mean effective stress (p').
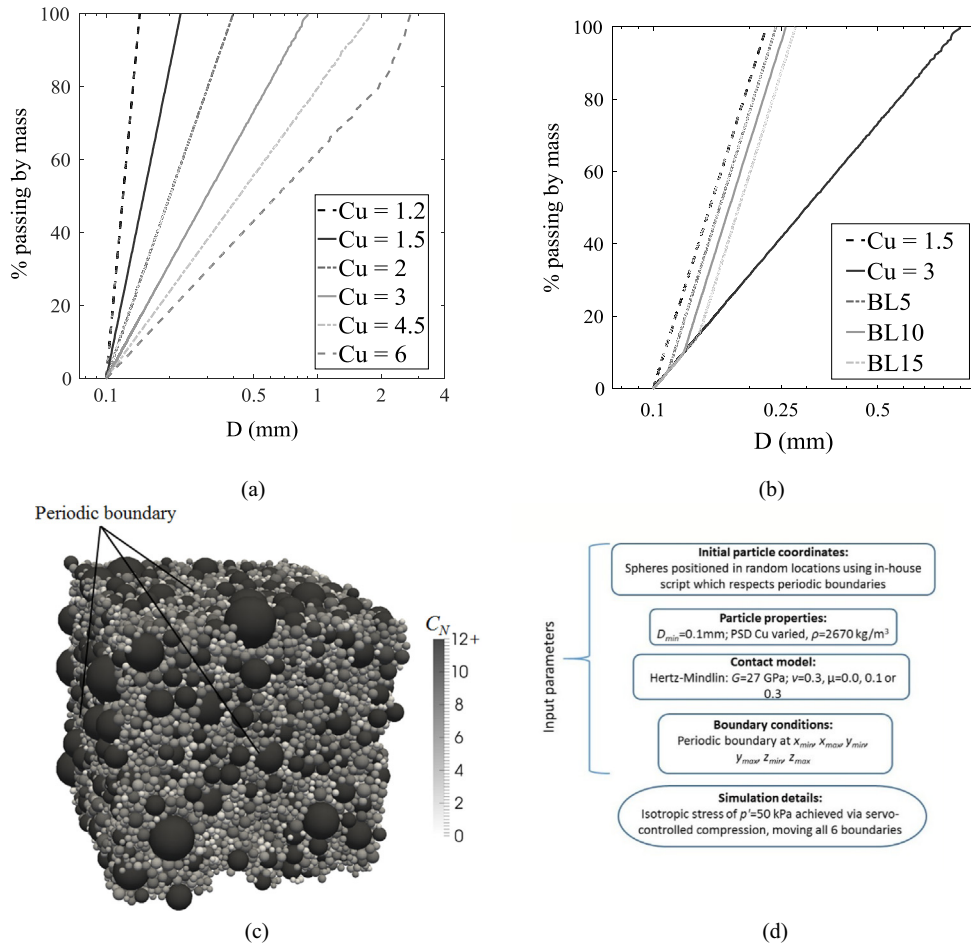

Fig. 5. Particle size distributions for polydisperse samples (a) linear gradings, (b) bi-linear gradings, (c) representative sample configuration ($Cu = 3$), and (d) simulation flow chart.

the contact data used to determine $\boldsymbol{K}$ were extracted at this point for eigenvalue analysis. These simulations were also used to generate data for a study on void constriction sizes [42,43]. The version of LAMMPS used for these simulations uses a fixed, user-defined time step and so the simulation time step was determined by considering the relationships proposed by Hart et al. [14] given as Eq. (2) above. The mass and stiffness of the smallest particle in the sys-

tem is used to calculate $\sqrt{\frac{m_{min}}{K_{max}}}$. The K_{max} value is predicted by considering the normal contact spring and assuming a maximum permissible particle overlap of 5% of the smallest diameter (note that in the simulations carried out here the actual overlaps do not exceed 1%). The simulation time step was then

$$\Delta t_{sim} = 0.05\sqrt{\frac{m_{min}}{K_{max}}} = 2.5 \times 10^{-9} \text{ s.}$$
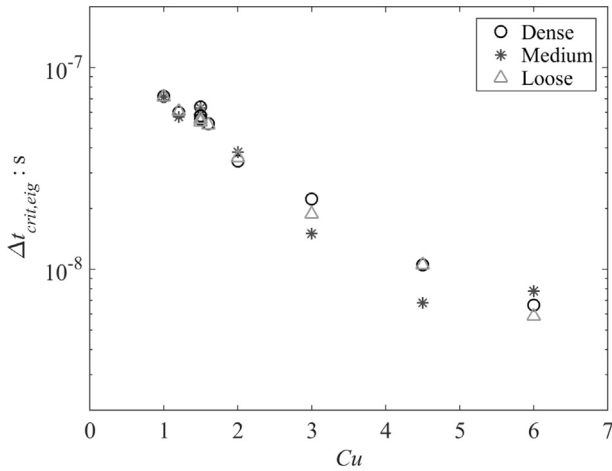
Fig. 6. variation in $\Delta t_{crit,eig}$ with Cu for polydisperse samples with D_{min} = 0.1 mm.

Referring to Fig. 6 the inferred $\Delta t_{crit,eig}$ values vary with Cu, despite having the same minimum particle diameter in all cases. The data are presented on a semi-logarithmic scale and the non-

linear nature of the relationships indicates that there is not a simple correlation between Δt_{crit} and Cu. Referring to Eq. (2) above, if the minimum mass is constant for all simulations, then Δt_{crit} should depend on $K_{N,max}$ and, as illustrated in Fig. 7(a), Δt_{crit} is indeed generally inversely proportional to $K_{N,max}$. As noted above, O'Sullivan and Bray [6] found that Δt_{crit} tended to decrease with coordination number C_N, and referring to Fig. 7b, plotting $\Delta t_{crit,eig}$ against the maximum per particle coordination number $C_{N,max}$ indicates that generally $\Delta t_{crit,eig} \propto C_{N,max}^{-\frac{2}{3}}$. The dependency of $\Delta t_{crit,eig}$ on both $K_{N,max}$ and $C_{N,max}$ prompted a regression analysis to determine the coefficients in an expression of the form $\Delta t_{crit,eig} = A(K_{N,max})^n (C_{N,max})^m$, giving $n = -0.379$ and $m = -0.412$. As $m \approx n$, Fig. 7c considers the variation in $\Delta t_{crit,eig}$ with the product $K_{N,max}C_{N,max}$ and good agreement is obtained with the plot indicating $\Delta t_{crit,eig} \propto (K_{N,max}C_{N,max})^{-0.4}$.

Considering all the DEM samples analyzed, the calculated $\Delta t_{crit,eig}$ were compared with selected estimates of Δt_{crit} using the approaches documented in the literature as noted above. The T_R values determined for all the simulations were calculated by applying Eq. (6) and Fig. 8a considers the variation in the ratio $\Delta t_{crit,eig}/T_R$ with $C_{N,max}$. Within the dataset considered here, for the low polydispersity samples with $C_{N,max} < 15$, $\frac{\Delta t_{crit,eig}}{T_R} > 1$ and
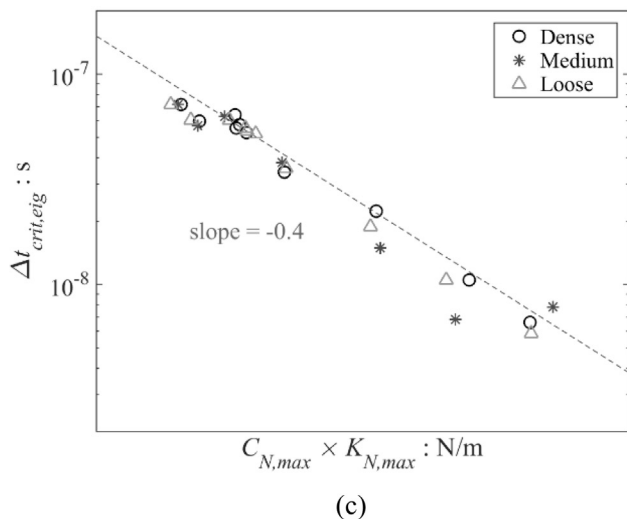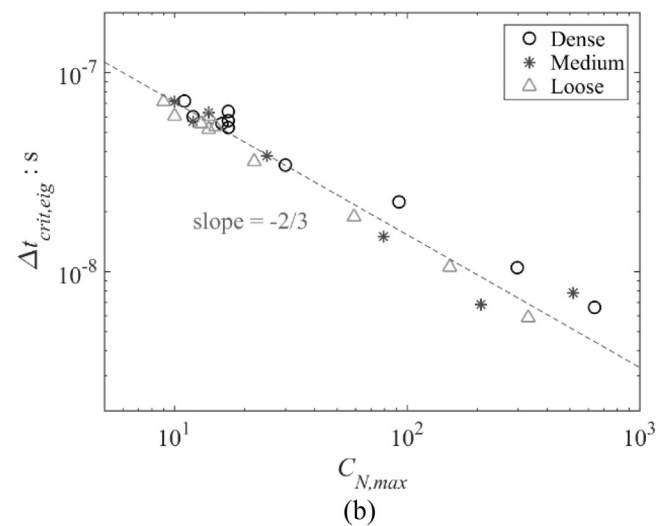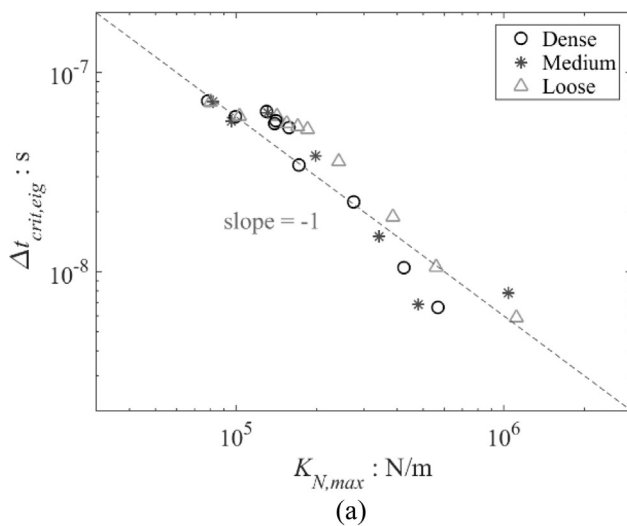
Fig. 7. $\Delta t_{crit,eig}$ values for polydisperse samples with D_{min} = 0.1 mm. (a) Variation in $\Delta t_{crit,eig}$ with maximum normal contact stiffness ($K_{N,max}$), (b) $\Delta t_{crit,eig}$ with maximum coordination number ($C_{N,max}$), and (c) variation in $\Delta t_{crit,eig}$ with $K_{N,max} \times C_{N,max}$.
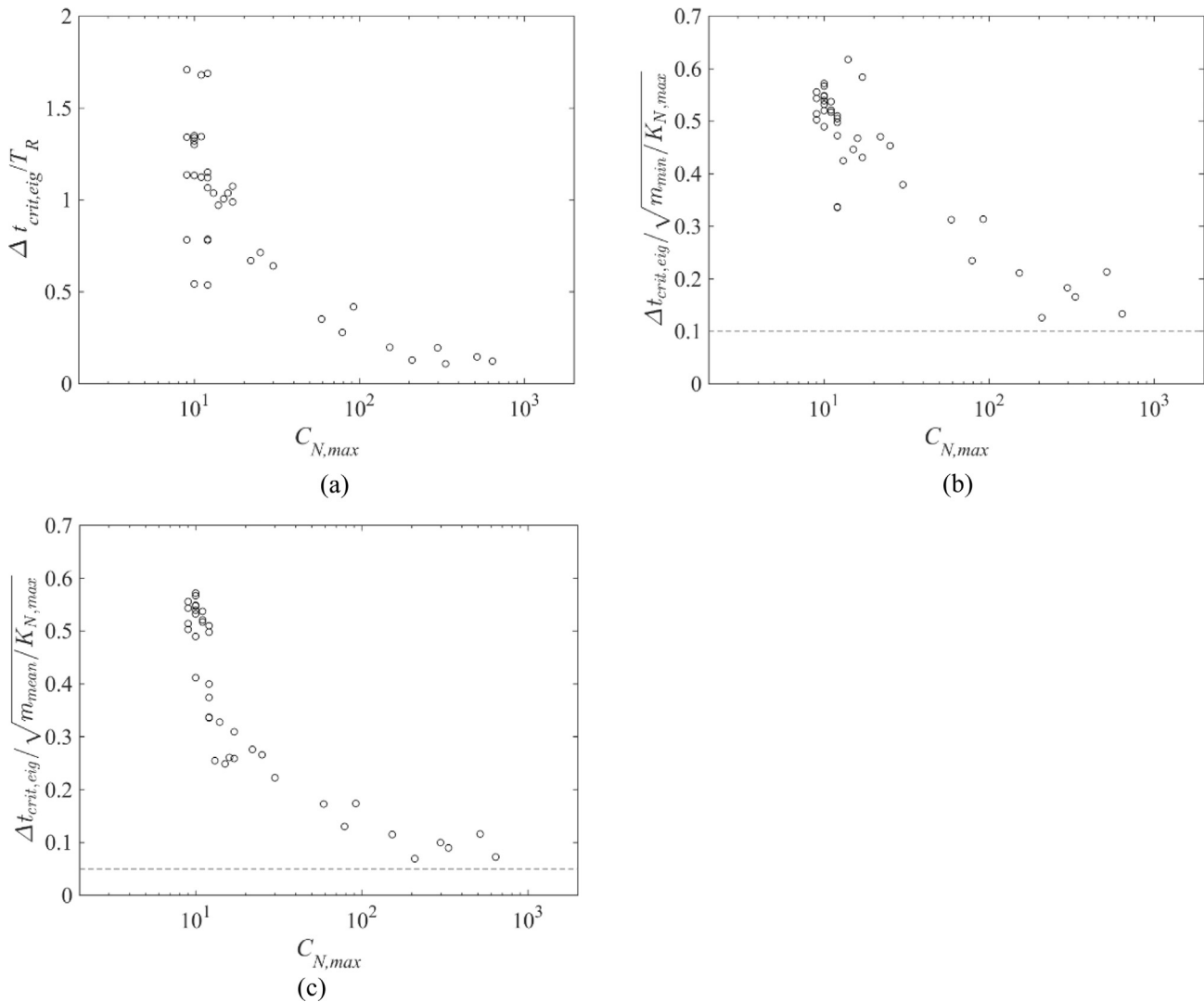
Fig. 8. Comparison of maximum coordination number with guidance given in literature (a) Variation in $\Delta t_{crit,eig}/T_R$ as a function of $C_{N,\max}$ (b) Variation in $\Delta t_{crit,eig}/\sqrt{m_{\min}/K_{N,\max}}$ as a function of $C_{N,\max}$ (c) Variation in $\Delta t_{crit,eig}/\sqrt{m_{mean}/K_{N,\max}}$ as a function of $C_{N,\max}$

use of $T_R = \Delta t_{crit}$ is generally appropriate at lower stress levels (<1 MPa); for these samples $Cu \leqslant 1.5$ and $R_{max}/R_{min} < 2.6$. (The data points with $\frac{\Delta t_{crit,eig}}{T_R} < 1$ and $C_{N,\max} < 15$ are associated with stress levels of 1 MPa or 10 MPa.) The time steps calculated using the eigenvalue approach are compared with the ratio $\sqrt{\frac{m_{min}}{K_{N,max}}}$ in Fig. 8b, where the ratio $\Delta t_{crit,eig}/\sqrt{\frac{m_{min}}{K_{N,max}}}$ is plotted against $C_{N,\max}$. These data indicate that $\Delta t_{crit,Tsuji} = 0.63\sqrt{\frac{m}{K_{N,max}}}$ is only slightly unconservative at low coordination number values, which would include the monodisperse samples considered by Tsuji et al. [15], however it significantly overestimates $\Delta t_{crit,eig}$ for polydisperse samples with maximum coordination numbers exceeding 10. For these polydisperse samples the Hart et al. [14] recommendation $\Delta t_{crit,Hart} = 0.14\sqrt{\frac{m_{min}}{K_{max}}}$ is more appropriate and the data presented here indicate that it can be argued that $\Delta t_{crit,safe} = 0.1\sqrt{\frac{m_{min}}{K_{max}}}$. Interestingly the scatter in the data is reduced if the ratio $\Delta t_{crit,eig}/\sqrt{\frac{m_{mean}}{K_{N,max}}}$ is considered as illustrated in Fig. 8c possibly reflecting the fact that the $K_{N,\max}$ and $C_{N,\max}$ are unlikely to be associated with the smallest particles as the smallest particles have less surface area to engage contacts and are more likely to transmit less

than average stresses [44]. However these data indicate that if m_{mean} is considered a more appropriate lower bound to the data is then given by $\Delta t_{crit,safe} = 0.05\sqrt{\frac{m_{mean}}{K_{max}}}$. These observations on lower limits to $\Delta t_{crit,safe}$ are however empirical and may not be generally applicable. They also significantly underestimate Δt_{crit} at lower $C_{N,\max}$ and in these cases use of this simple ratio-based approach that neglects consideration of the contact conditions can lead to a significant waste of computing time/resources. Burns and Hanley [7] also noted the potential for erroneous calculation of Δt_{crit} to lead to computational inefficiency. The overall observation that the critical time increment depends on mass, contact spring stiffness and the maximum coordination number supports the use of more sophisticated approaches such as those based on Gerschgorin's theorem adopted by Serra et al. [20] and Itasca [19] that account for variations in coordination number.

Building on the correlations observed in Figs. 3c, 4c, 6, 7 and 8 all of the data presented here were combined to develop a simple expression relating the critical time increment to parameters that can be efficiently checked in a DEM simulation. Fig. 7c indicates $\Delta t_{crit,eig} \propto (K_{N,max}C_{N,max})^{-0.4}$ and this observation is combined with the Hart et al. [14] recommendation by considering the ratio $\sqrt{\frac{m_{min}}{K_{N,max}C_{N,max}}}$. Referring to Fig. 9a and c $\sqrt{\frac{m_{min}}{K_{N,max}C_{N,max}}}$ seems to give a
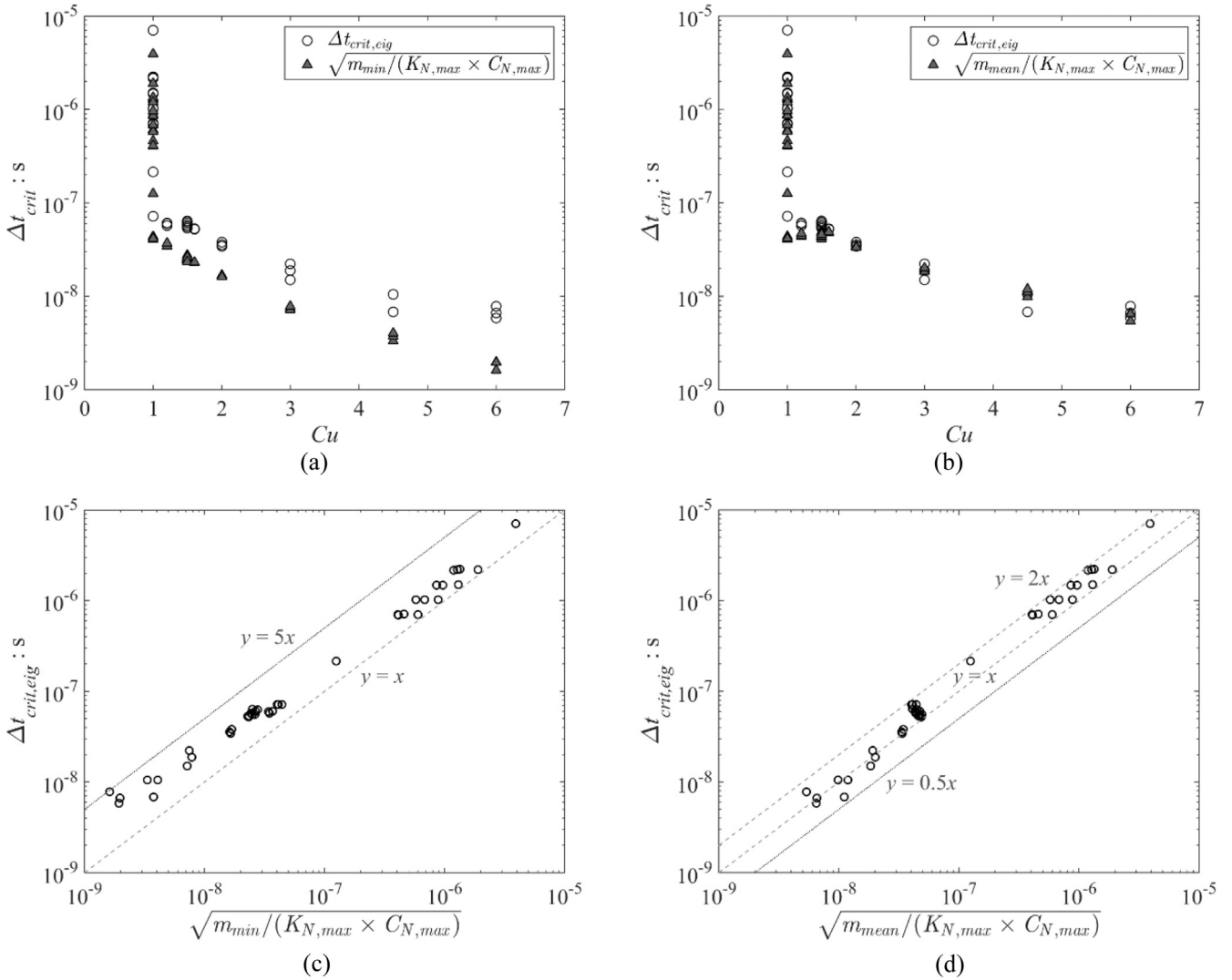
Fig. 9. Best-fit expressions for $\Delta t_{crit,eig}$ based on current dataset (a) Variation in $\Delta t_{crit,eig}$, and correlation based on the minimum mass (m_{min}) with Cu (b) Variation in $\Delta t_{crit,eig}$, and correlation based on m_{mean} with Cu (c) $\Delta t_{crit,eig}$ correlation using m_{min} (d) $\Delta t_{crit,eig}$ correlation using m_{mean}

lower bound to the observed $\Delta t_{crit,eig}$; use of this expression may however be overly conservative as it can give values as low as $0.2\Delta t_{crit,eig}$. As was observed in Fig. 8c the scatter in the data is reduced if $\sqrt{\frac{m_{mean}}{K_{N,max}C_{N,max}}}$ is considered, however in this case the ratio $\sqrt{\frac{m_{mean}}{K_{N,max}C_{N,max}}}$ can be unconservative and over estimate $\Delta t_{crit,eig}$ (Fig. 9b and d). The data presented in Fig. 9 and the associated ratios are likely useful to DEM analysts as they give estimates of Δt_{crit} and illustrate the extent of the sensitivity of the critical time step to the packing density as quantified by $C_{N,max}$. It is important to realize however that these data are limited in extent; a finite number of DEM samples were considered and the generality of the applicability of the expressions fitted to the data is not proven as they are empirically-derived.

6. Conclusion

This contribution has extracted mass and contact stiffness information from DEM simulations to construct system (global) mass and stiffness matrices. Eigenvalue decomposition of these matrices was used to determine the maximum frequency in the system from which the critical time step could be directly determined. The eigenvalue decomposition approach was validated by compar-

ison with the analytical expressions developed by O'Sullivan and Bray [6] and simulations of triaxial compression of samples of uniform spheres with a face-centered cubic packing. To assess how a DEM model's characteristics affect the critical time increment Δt_{crit}, three DEM datasets were considered (i) monodisperse samples at a constant mean effective stress but with varying particle diameters (ii) monodisperse samples where the mean effective stress was varied and (iii) polydisperse samples where the particle size distribution was systematically varied at a constant mean effective stress. The following conclusions are made:

1. Broadly three approaches to calculating Δt_{crit} are documented in the literature. The first uses the oscillation period of a single degree of freedom system as a basis to calculate Δt_{crit}; while the second, which is applied when a Hertzian contact model is used, considers the Rayleigh wave speed. The third uses slightly more complex implementations based on Gerschgorin's theorem, and can account for non-linear contact models and consider the number of contacts involving each particle.
2. The results obtained by considering triaxial compression of a face-centered cubic assembly and systematically varying the DEM simulation time step support the recommendation of Belytchko et al. [12] that the critical time increment obtained

from the eigenvalue decomposition be multiplied by a factor <0.9 to obtain a safe estimate of Δt_{crit}. These data also highlight the benefits of tracing the energy balance in the numerical model to identify instabilities.

3. Where the Hertzian contact model is used and the mean effective stress remains constant, the critical time step is directly proportional to the particle diameter for monodisperse systems. The validity of this observation based on eigenvalue decomposition was confirmed by considering effective medium theory.

4. For monodisperse systems there can be a threefold variation in Δt_{crit} over the range of stresses that might be considered in geomechanical analyses (i.e. from 10 kPa to 10 MPa). This variation is not captured where the Rayleigh wave speed approach is used to determine Δt_{crit}.

5. For the polydisperse systems with linear and bi-linear particle size distributions considered here with $Cu \leqslant 6$ there was a twelve-fold variation in the calculated critical time increment as the degree of polydispersity increased. This variation is not captured where the Rayleigh wave speed approach is used to determine Δt_{crit} using the minimum mass. From consideration of these samples it is clear that Δt_{crit} depends on the contact stiffness, minimum particle mass and the coordination number. This confirms the analytical finding of O'Sullivan and Bray [6] and supports the approach of Itasca [19] which includes a summation of contacts for each particle. It is interesting to note that it is the maximum particle coordination number that specifically influences Δt_{crit}.

6. An overall synthesis of the data from the three series of simulations indicates that using the Rayleigh wave speed approach (T_R) is valid only at low stress levels where the maximum coordination number is less than 15. The relationship between the calculated Δt_{crit} and the ratios $\sqrt{\frac{m_{mean}}{K_{max}}}$ and $\sqrt{\frac{m_{min}}{K_{max}}}$ supports use of the expression $\Delta t_{crit,safe} = 0.05\sqrt{\frac{m_{mean}}{K_{max}}}$ or $0.1\sqrt{\frac{m_{min}}{K_{max}}}$ to give a conservative estimate of Δt_{crit}. Note however that where these expressions are used in systems with low maximum coordination numbers they can result in very small time steps that are over conservative and thus cause unnecessary increases in the computational cost of DEM simulations; as researchers move towards larger simulations and use large tier 1 and tier 0 high performance computers there is potential for a significant waste of resources and energy. Consequently the computational overhead cost associated with using approaches based on Gerschgorin's theorem to recalculate the critical time increment on an ongoing basis during a simulation will be justified in many cases.

7. Considering the dataset as a whole, it seems that expressions of the form $\sqrt{\frac{m_{min}}{K_{N,max}C_{N,max}}}$ or $\sqrt{\frac{m_{mean}}{K_{N,max}C_{N,max}}}$ can be used to approximate Δt_{crit}. It is straightforward in a DEM code to track $K_{N,max}$ and $C_{N,max}$ and so these expressions in this form could adopted with no significant computational cost. At the start of a simulation when $K_{N,max}$ and $C_{N,max}$ are not known reasonable predictions might be made or it might be possible to use T_R with a conservative "safety factor" to get an initial estimate. These expressions also enable DEM analysts to better understand how the characteristics of the particular system affect Δt_{crit} and the computational cost of the simulations. Note however that these expressions are empirical and were developed considering a finite number of DEM simulations; the general applicability to DEM models with characteristics that differ from those samples considered here is not demonstrated.

8. The observations presented here are based on analysis of DEM samples, rather than a theoretical/analytical study of stability. The study is empirical, the results are developed from an analysis of selected DEM data sets and so the general applicability of

the quantitative correlations and observations to all DEM simulations is unproven. The data clearly support the application and development of approaches to calculate Δt_{crit} that can account for the dependencies highlighted here. We acknowledge that there may be a computational cost associated with implementing such methods; however, as highlighted here use of very simple approaches can result in simulations either being unstable or having an unjustifiably high computational cost.

Acknowledgements

References

[1] O'Sullivan C. Particulate discrete element modelling – a geomechanics perspective. Taylor and Francis; 2011.

[2] Zhu HP, Zhou ZY, Yang RY, Yu AB. Discrete particle simulation of particulate systems: theoretical developments. Chem Eng Sci 2007;62:3378–96. http://dx.doi.org/10.1016/j.ces.2006.12.089.

[3] Zhu HP, Zhou ZY, Yang RY, Yu AB. Discrete particle simulation of particulate systems: a review of major applications and findings. Chem Eng Sci 2008;63:5728–70. http://dx.doi.org/10.1016/j.ces.2008.08.006.

[4] Potyondy DO, Cundall PA. A bonded-particle model for rock. Int J Rock Mech Min Sci 2004;41:1329–64.

[5] Hanley K, O'Sullivan C. Analytical study of the accuracy of discrete element simulations. Int J Numer Methods Eng 2016;55:947–71. http://dx.doi.org/10.1002/nme.5275.

[6] O'Sullivan C, Bray JD. Selecting a suitable time step for discrete element simulations that use the central difference time integration scheme. Eng Comput 2003;21:278–303. http://dx.doi.org/10.1108/02644400410519794.

[7] Burns SJ, Hanley KJ. Establishing stable time-steps for DEM simulations of non-collinear planar collisions with linear contact laws. Int J Numer Methods Eng 2016. http://dx.doi.org/10.1002/nme.5361.

[8] Plimpton S. Fast parallel algorithms for short-range molecular-dynamics. J Comput Phys 1995;117:1–19.

[9] Kloss C, Goniva C, Hager A, et al. Models, algorithms and validation for opensource DEM and CFD-DEM. Prog Comput Fluid Dyn An Int J 2012;12:140–52.

[10] Smilauer V, Catalano E, Chareyre B, et al. Yade documentation. The Yade Project; 2010. , http://yade-dem.org/doc/.

[11] Itasca Consulting Group. PFC3D version 4.0 user manual. Minneapolis (MN, USA): Itasca Consulting Group; 2007.

[12] Belytschko T, Liu WK, Moran B. Nonlinear finite elements for continua and structures. John Wiley; 2000.

[13] Cundall Pa, Strack ODL. A discrete numerical model for granular assemblies. Géotechnique 1979;29:47–65. http://dx.doi.org/10.1680/geot.1979.29.1.47.

[14] Hart R, Cundall PA, Lemos J. Formulation of a three-dimensional distinct element model—Part II. Mechanical calculations for motion and interaction of a system composed of many polyhedral blocks. Int J Rock Mech Min Sci Geomech Abstr 1988;25:117–25. http://dx.doi.org/10.1016/0148-9062(88)92294-2.

[15] Tsuji Y, Kawaguchi T, Tanaka T. Discrete particle simulation of a two-dimensional fluidized bed. Powder Tech 1993;77:79.

[16] Johnson K. Contact mechanics. Cambridge (UK): Cambridge University Press; 1985.

[17] Jensen A, Fraser K, Laird G. Improving the precision of discrete element simulations through calibration models. In: 13th Int LS-DYNA users conf. p. 1–12.

[18] Tu X, Andrade JE. Criteria for static equilibrium in particulate mechanics computations. Int J Numer Methods Eng 2008;75:1581–606. http://dx.doi.org/10.1002/nme.2322.

[19] Itasca Consulting Group. Mechanical timestep determination. PFC 5.0 Doc; 2014.

[20] Serra C, Azevedo NM, Batista AL. Code implementation of particle based discrete element method for concrete viscoelastic modelling, vol. 74; 2015.

[21] Underwood P. Dynamic relaxation. Comput Methods Transient Anal Comput Methods Mech Ser, vol. 1. Elsevier; 1983. p. 245–65.

[22] Boac JM, Ambrose RPK, Casada ME, et al. Applications of discrete element method in modeling of grain postharvest operations. Food Eng Rev 2014;6:128–49. http://dx.doi.org/10.1007/s12393-014-9090-y.

[23] Li Y, Xu Y, Thornton C. A comparison of discrete element simulations and experiments for "sandpiles" composed of spherical particles. Powder Technol 2005;160:219–28. http://dx.doi.org/10.1016/j.powtec.2005.09.002.

[24] Thornton C. Numerical simulations of deviatoric shear deformation of granular media. Géotechnique 2000;50:43–53. http://dx.doi.org/10.1680/geot.2000.50.1.43.

[25] Thornton C, Randall C. Applications of theoretical contact mechanics to solid particle system simulation. In: Satake M, Jenkins JT, editors. Micromech Granul Matter. Elsevier; 1988. p. 133–42.

[26] Marigo M, Stitt EH. Discrete element method (DEM) for industrial applications: comments on calibration and validation for the modelling of cylindrical pellets. KONA Powder Part J 2015;32:236–52. http://dx.doi.org/10.14356/kona.2015016.

[27] Kremmer M, Favier JF. A method for representing boundaries in discrete element modelling—part II: Kinematics. Int J Numer Methods Eng 2001;51:1423–36. http://dx.doi.org/10.1002/nme.185.

[28] Kafui KD, Thornton C, Adams MJ. Discrete particle-continuum fluid modelling of gas-solid fluidised beds. Chem Eng Sci 2002;57:2395–410. http://dx.doi.org/10.1016/S0009-2509(02)00140-9.

[29] Guo Y, Wassgren C, Hancock B, et al. Validation and time step determination of discrete element modeling of flexible fibers. Powder Technol 2013;249:386–95. http://dx.doi.org/10.1016/j.powtec.2013.09.007.

[30] Boac JM, Casada ME, Maghirang RG, Harner III JP. 3-D and quasi-2-D discrete element modeling of grain commingling in a bucket elevator boot system. Trans ASABE 2012;55:659–72. http://dx.doi.org/10.13031/2013.41367.

[31] Lopera Perez JC, Kwok CY, O'Sullivan C, et al. Assessing the quasi-static conditions for shearing in granular media within the critical state soil mechanics framework. Soils Found 2016;56:152–9. http://dx.doi.org/10.1016/j.sandf.2016.01.013.

[32] da Cruz F, Emam S, Prochnow M, et al. Rheophysics of dense granular materials: discrete simulation of plane shear flows. Phys Rev E 2005;72:021309. http://dx.doi.org/10.1103/PhysRevE.72.021309.

[33] Ke T, Bray J. Modeling of particulate media using discontinuous deformation analysis. J Eng Mech 1995;121:1234–43. http://dx.doi.org/10.1061/(ASCE)0733-9399(1995) 121:11(1234).

[34] Sack RL. Matrix structural analysis. Waveland Press; 1989.

[35] Zienkiewicz OC, Taylor RL. The finite element method. The Basis, vol. 1. Butterworth Heinemann; 2000.

[36] Belytschko T. An overview of semidiscretization and time integration procedures. In: Computational methods in mechanics series. Comput Methods Transient Anal, vol. 1.

[37] Hughes TJR. Transient algorithms and stability. Comput Methods Transient Anal Comput Methods Mech Ser 1983;1.

[38] Otsubo M, O'Sullivan C, Hanley KJ, Way Sim Way. Influence of packing density and stress on the dynamic response of granular materials. Granul Matter 2017 (accepted for publication).

[39] Thornton C. The conditions for failure of a face-centered cubic array of uniform rigid spheres. Géotechnique 1979;29:441–59. http://dx.doi.org/10.1680/geot.1979.29.4.441.

[40] Yimsiri S, Soga K. Micromechanics-based stress-strain behaviour of soils at small strains. Géotechnique 2000;50:559–71. http://dx.doi.org/10.1680/geot.2000.50.5.559.

[41] Gonzalez D Barreto. Numerical and experimental investigation into the behaviour of granular materials under generalised stress states. University of London; 2009.

[42] Shire T. Micro-scale modelling of granular filters. Imperial College London; 2014.

[43] Shire T, O'Sullivan C. Constriction size distributions of granular filters: a numerical study. Géotechnique 2016;66:826–39. http://dx.doi.org/10.1680/jgeot.15.P.215.

[44] Shire T, Sullivan CO, Hanley KJ, Fannin RJ. Fabric and effective stress distribution in internally unstable soils. J Geotech Geoenviron Eng 2014;140:1–11. http://dx.doi.org/10.1061/(ASCE)GT.1943-5606.0001184.